Mountain Hydrology: Slope-aspect Effects on snow-insulation timing and ground temperatures

Carlos Pineda, University of Washington
Mentors: Jessica Lundquist, Rosemary Carroll, and Ethan Gutmann

Full-time independent research/REU

2026

Abstract

Slope and aspect are major sources of topographic heterogeneity in mountain watersheds because they influence the amount and timing of incoming solar radiation. These differences affect snow accumulation, snow disappearance, and the thermal conditions of soils. This study examines snow-insulation and disappearance timing at 19 north- and south-facing monitoring sites near the Rocky Mountain Biological Laboratory in the East River watershed, Colorado. Near-surface ground-temperature measurements collected at 30-minute intervals during Water Years 2024–2026 were used to classify days as deep snow, shallow or patchy snow, or snow-free. Site characteristics derived from spatial datasets included elevation, slope, aspect, diurnal anisotropic heating index, topographic position, canopy cover, and modeled terrain shading. During Water Year 2026, the median snow-insulation end date was April 6 at south-facing sites and May 7 at north-facing sites, indicating that insulating snow conditions ended approximately one month earlier on south-facing slopes. However, the median shallow or patchy snow period was 28.5 days longer at south-facing sites than at north-facing sites. Snow-insulation end dates also showed greater variability during Water Year 2026 than during the two preceding water years. These results demonstrate that slope and aspect influence both the timing of snow-insulation loss and the duration of transitional snow conditions, while local elevation, vegetation, and terrain shading contribute additional variability among sites.

Introduction

Snow provides fundamental resources in the form of water in vast parts of the world (Sturm et al., 2017). In the western United States, approximately 53% of annual runoff is derived from snow, while in mountainous regions such as the Rocky Mountains, Sierra Nevada, and the Cascades, snow contributes more than 70% of annual streamflow (Li et al., 2017). As a result, the timing and magnitude of snow accumulation and melt play a crucial role in determining water availability for ecosystems, agriculture, hydropower, and human consumption (Sturm et al., 2017).

Recent observations have highlighted growing inconsistencies between snowpack and streamflow. For example, in 2021 the Colorado River Basin experienced snowpack conditions near 80% of average, yet generated less than 30% of average streamflow (Fleck & Udall, 2021). While rising temperatures are known to reduce the fraction of snowmelt that ultimately contributes to runoff (Berghuijs et al., 2014; Milly & Dunne,2020; Modi et al., 2022), substantial uncertainty remains regarding the processes responsible for these discrepancies. Current hydrologic models often diverge in their sensitivity to warming (Vano et al., 2012) because they struggle to represent local-scale heterogeneity, including groundwater interactions, soil moisture dynamics, and spatial variability in snow cover (Fan, 2019; Kampf, 2020; Gordon et al.,2022; Cho et al., 2022).

Understanding how local heterogeneities influence snowmelt processes is therefore essential for improving hydrologic predictions under a changing climate. One important source of heterogeneity is slope aspect, the cardinal direction a hillslope faces. Aspect strongly influences incoming solar radiation, resulting in differences in snow accumulation, snowmelt timing, and surface energy balance. South-facing slopes in the Northern Hemisphere generally receive more solar radiation than north-facing slopes, causing snow to disappear earlier and exposing soils to atmospheric heating sooner in the season (Lundquist & Flint, 2006). However, less attention has been given to the consequences of earlier snow disappearance for near-surface environmental conditions, including near-surface soil temperatures. Because snow acts as an insulating layer, its disappearance exposes soils to larger temperature fluctuations and increased solar heating and therefore, ground temperature measurements are a reliable way to determine snow presence (Slater et al., 2017, Lundquist & Lott, 2015).

The 2025–2026 water year provides a unique opportunity to investigate these relationships. Historical snow depth and snow water equivalent records indicate that Water Year 2026 was among the lowest snowpack years in the observational record (Butte SNOTEL). Using near-surface soil temperature sensors from monitoring sites across the East River watershed, this study examines how slope aspect influences snow-insulation timing and ground-temperature responses. Specifically, we ask: (1) Does snow insulation end earlier on south-facing slopes than on north-facing slopes? (2) Do south-facing slopes experience shorter zero-curtain periods, the time period where ground temperatures remain between -0.5°C and 0.5°C, and later freezing onsets? and (3) How did the timing and variability of snow-insulation loss during the low-snow Water Year 2026 compare with Water Years 2024 and 2025? We hypothesize that south-facing sites lose snow insulation earlier, experience shorter zero-curtain periods and later freezing onsets, and display greater differences from north-facing sites during Water Year 2026 compared to more typical years.

Data and Methods

Study Area and Experimental Site

The study took place in the East River watershed, which is centered at (38° N-40°N, -107° W) northeast of Crested Butte, Colorado. The watershed contains strong variation in elevation, slope, aspect, vegetation, shading, and topographic position. Existing observation locations are distributed among the Avery Peak (38°N, -106°W), Rustlers Gulch (39°N,-106°W), Kettle Ponds (38.9°N,-106.9°W), and Emerald Lake (39°N,-107°W) areas (Figure 1). Monitoring sites were arranged along transects, spanning from north-facing to south-facing sides of the valley. There are seven monitoring sites in a transect near Avery Peak labeled AP1-AP7, five monitoring sites across Rustlers Gulch labeled R1-R5,and six monitoring sites across Kettle Ponds labeled KP1-KP6, as well as one monitoring site in Emerald Lake labeled EL2. Monitoring of the AP, KP, and EL sites started in the Water Year of 2024, while monitoring at the RG sites started in the Water Year of 2025.

At each site there are three types of quantitative measurements being taken: air temperature, relative humidity, and ground temperature. The air temperature and relative humidity measurements are taken by a HOBO Temperature/RH Data Logger every 30 minutes. This sensor is positioned underneath a tree's shade cover so that solar radiation does not affect its measurements. This method has been demonstrated to work better than an unaspirated radiation shield (Lundquist and Lott 2008). The ground temperature measurement is taken every 30 minutes by a HOBO Pendant MX Water Temperature Data Logger. Ground sensors were positioned approximately 2 cm below the surface, generally next to a very small tree or bush, within 2 m of the air temperature sensor. Ground temperature measurements were key to this study because snow serves as an insulating system, whereas snow falls and it accumulates it insulates the ground underneath. Thus ground temperature measurements allow us

Precarious Peak and the other one located at the RG5 site facing north. Furthermore, there are two cameras at the Kettle Ponds sites, one is located at the KP1 site which points to Snodgrass/KP5 and KP6, the second camera is located at the KP5 location observing the KP1-KP2 sites. Finally, there is one camera located at the Emerald Lake site which observes Maroon Belles.

Some of the limitations when collecting data were loss of data due to tampering of the data logger at the RG5 site in 2026, where the ground temperature sensor was unburied and took measurements of near-surface temperature (Figure 2), and the air temperature and relative humidity sensor most likely suffered water damage from a rupture in the sensor.

Methods

Slope Gradient and Aspect Calculation

Topographic characteristics at each site were determined following algorithms and techniques detailed in Jiang et al., 2026 and Cristea et al., 2017.

Site-specific slope gradient and aspect were determined from a 3-meter Digital Elevation Model (DEM), using terrain analysis tools in QGIS 3.44 following Jiang et al., 2026. Surface elevation gradients were estimated using the 3 x 3 weighted moving algorithm in Jiang et al., 2026. The algorithm computes the east-west gradient and north south gradient using the elevation values of neighboring cells within a 3 x 3 window centered on the target cell:

$$\frac{\partial z}{\partial x} = \frac{[(z_3+2z_6+z_9)-(z_1+2z_4+z_7)]}{8 \times L}$$

$$\frac{\partial z}{\partial y} = \frac{[(z_7+2z_8+z_9)-(z_1+2z_2+z_3)]}{8 \times L}$$

where z_1 to z_9 represent the elevation values of the nine grid cells within the 3 × 3 window (numbered from top left to bottom right), and L is the grid resolution. The slope angle (θ), which represents the maximum rate of spatial change in surface elevation, was calculated from the gradient as follows:

$$\theta = arctan[\sqrt{(\frac{\partial z}{\partial x})^2 + (\frac{\partial z}{\partial y})^2}] \times \frac{180°}{\pi}$$

This method yields the three-dimensional slope angle, which represents the inclination of the steepest descent direction at each point, rather than a two-dimensional projection along any specific direction.
The aspect (α) is defined as the azimuth of the downslope vector (measured clockwise from north, ranging from 0° to 360°) and is calculated using the four-quadrant arctangent function as follows:

$$\alpha = [arctan2(-\frac{\partial z}{\partial x}, -\frac{\partial z}{\partial y})\frac{180°}{\pi} + 360°]mod\,360°$$

Aspect values ranged from 0° to 360°, with 0°representing north, 90° east, 180° south, and 270° west. Aspect was treated as undefined where slope was less than 0.001°. Calculations were performed only for cells with complete, valid 3 × 3 neighborhoods.

Heating Index Calculation

Using the formula from Cristea et al., 2017, the diurnal anisotropic heating index [*Böhner and Antonić*, 2009], used to represent ablation effect at each site was calculated as follows using the slope angle (θ) and the aspect (α):

$$DAH = cos(\alpha_{max} - \alpha) \times arctan(\theta)$$

Where $\alpha_{max} = 202.5°$(SSW) is the slope aspect receiving the maximum amount of solar radiation. It is known from previous research that south facing slopes have a higher DAH than north facing slopes. This index ranges from -1 to 1, thus south facing slopes will have a DAH closer to 1, flat slopes have a value of 0 ,and north facing slopes will have a value closer to -1. The DAH was used to determine the relative amount of solar radiation a specific site receives and served as one of the factors when comparing snow disappearance date and rise in ground temperatures.

Topographic Position Index

The topographic position index is a measure of the concavity of a specific site. Its value determines whether a pixel is located in a depression or on a ridge. It is calculated as follows:

$$TPI = z_0 - \bar{z},\ with\ \bar{z} = \frac{1}{n_R}\sum_{i \in R} z_i$$

Where z_0 is the elevation of the given cell and $\bar{z}$ is the mean elevation of the neighboring cells in the set R.

Canopy and topographic shading

Vegetation and topographic shading were characterized separately. Proportional canopy cover at each monitoring site was obtained from a 9 m spatial-resolution LiDAR-derived canopy-cover raster found in the Rocky Mountain Biology Laboratory data hub. Canopy cover was calculated for each 9 m grid cell as the proportion of discrete laser returns located between 2 and 45 m above the ground surface. Raster values ranged from 0, representing no canopy cover, to 1, representing complete canopy cover. Proportional values were multiplied by 100 for reporting as percent canopy cover.

Surrounding topographic shading was extracted from 30m terrain-shading rasters, which were prepared as inputs for the Distributed Hydrology Soil Vegetation Model (DHSVM). For each raster cell, the surrounding terrain was used to construct an upward-looking representation of the local horizon. This was done by tracing the terrain in multiple azimuth directions and determining the maximum horizon angle, thereby identifying which portions of the sky were visible and which were obstructed by nearby ridges and mountains. ArcGIS solar-radiation methods represent this information as a hemispherical viewshed. A corresponding sun map describes the modeled position of the sun, including its azimuth and elevation, for a specified latitude, day of year, and time of day. The sun map is compared with the terrain viewshed to determine whether the direct solar beam reaches a cell or is blocked by surrounding terrain. Local slope and aspect affect the orientation of the land surface, while the horizon angles determine whether the sun is obstructed.

Each monthly raster contained 24 bands representing hourly terrain-shadow conditions for the 15th day of the month. For each monitoring site, values were extracted from the raster cell containing the site. Daylight intervals were defined as hourly bands in which at least one raster cell within the watershed had a positive value. A site was considered exposed to direct sunlight during an interval when its extracted raster value was greater than zero. Monthly terrain exposure was then calculated as the number of sunlit intervals divided by the total number of modeled daylight intervals. Therefore, this metric represents the proportion of potential daylight hours during which direct sunlight was not obstructed by terrain. It does not represent measured solar radiation and does not account for clouds or short-term atmospheric conditions.

Snow Presence

Snow conditions were inferred from the damping effect of insulating snow on ground-temperature variability. Raw ground-temperature measurements were recorded at 30-minute intervals and aggregated to daily minimum, maximum, mean, and range values. A day was considered valid when at least 36 of the expected 48 measurements were available. Missing observations were not interpolated, and duplicate timestamps were removed before daily aggregation.

Snow conditions were classified using a two-stage temperature-range algorithm. First, snow presence was determined using the trailing 48-hour ground-temperature range, calculated from the maximum and minimum temperatures observed during the current day and previous day. Both days were required to contain valid data. A day was classified as snow-covered when the 48-hour temperature range was less than or equal to 1°C, following Raleigh et al. 2013. A day was classified as snow-free when the 48-hour temperature range exceeded 1°C.

Snow-covered days were subsequently separated into deep-snow and shallow or patchy-snow conditions using the trailing 5-day ground-temperature range, calculated from the maximum and minimum temperatures observed during the current day and the previous four days. Three days were required to classify a snow day to account for days at the beginning of the record. A snow-covered day was classified as deep snow when the 5-day temperature range was less than or equal to 1.5°C and maximum ground temperatures remained between −0.5°C and 0.5°C. Snow-covered days with a 5-day range greater than 1.5°C and a minimum temperature below -0.5°C or a maximum temperature above 0.5°C were classified as shallow or patchy snow. Days lacking the required valid 48-hour or 5-day history were classified as having insufficient data or insufficient temporal history.

The snow-insulation end date was defined as the final day classified as deep snow. The snow-disappearance date was defined as the final day with inferred snow presence, including deep-snow, shallow or patchy-snow, and snow-present days for which the 5-day classification history was incomplete. Shallow or patchy-snow duration was calculated as the difference between the snow-disappearance date and the snow-insulation end date.

Ground Temperature Response

Following Jiang et al. (2026), the freeze–thaw process was characterized using daily mean ground temperature. Freezing onset was defined as the first date on which daily mean ground temperature fell below 0°C. Thawing onset was defined as the final transition above after which daily mean ground temperature did not fall below 0°C again. The zero-curtain period was defined as the longest uninterrupted sequence of days during which daily mean ground temperature remained between -0.5°C and 0.5°C, following Chen et al. (2021), Gao et al. (2018), and Quinton and Baltzer (2013). Zero-curtain duration was calculated as the number of days in this continuous period.

Interannual comparison

Interannual comparisons were conducted using records from WY2024, WY2025, and WY2026. Avery Peak, Kettle Ponds, and Emerald Lake had records for all three water years, whereas Rustler Gulch had records only for WY2025 and WY2026. The same snow-classification algorithm was applied to each site and water year. Snow-insulation end dates and freezing-onset dates were represented as day of year. For each water year and aspect class, the median and interquartile range were calculated. The interquartile range was defined as the difference between the 75th and 25th percentiles and represented the spread of the middle 50% of sites.

Results

Topographic Characteristics of Study Sites

A total of 19 sites were observed across the East River watershed, 9 north-facing and 10 south-facing. Site elevations ranged from 2790m to 3480m. Most sites had positive TPI values, indicating that they were generally elevated relative to their surrounding 90-m neighborhood. South-facing sites had a greater DAH index than north-facing sites.

Vegetation and topographic shading

Canopy cover varied substantially among the 19 monitoring sites, ranging from 3.0% at AP3 to 78.4% at KP5, with a median of 35.5% (Figure 4). The highest canopy cover occurred at KP5, AP6, and RG5, where cover exceeded 70%. In contrast, AP3, RG1, RG2, and AP4 had less than 10% canopy cover. These results demonstrate considerable variation in local vegetation cover across the monitoring network.

Modeled direct-sun exposure also varied among sites and throughout the year (Figure 5). Most sites received modeled direct sunlight during approximately 70–95% of the evaluated daylight intervals in most months. RG1, AP3, and AP6 generally had among the highest mean monthly exposure, whereas RG5 was consistently the most terrain-shaded site. At RG5, modeled direct-sun exposure declined to 27% in November and 0% in both December and January. Some sites displayed strong seasonal variation; for example, EL2 increased from 60–67% exposure during January and February to 94–100% from May through August before declining again during autumn and winter.

Sites Characteristics Relationship to Snowmelt timing

After evaluating the relationship between topographic characteristics and snow insulation timing, aspect and DAH each explained approximately 41% of the variation. Elevation explained only about 13% of the variation, while canopy cover, slope, TPI, and terrain exposure each explained 5% or less.

Snow insulation and disappearance timing

The earliest snow insulation end date for north-facing slopes was 7 March 2026, while the earliest snow insulation end date for south-facing slopes was 28 February 2026. The latest insulation end dates were 24 May 2026 and 15 May 2026, for north-facing and south-facing slopes, respectively. The median snow insulation end date for north-facing slopes was 07 May 2026, and was 06 April 2026 for south-facing slopes, representing a 31 day difference between median snow insulation date between north and south facing slopes. The median shallow/patchy snow period was 28.5 days longer at south-facing sites than at north-facing sites, where north facing slopes had a median shallow snow period of 1.0 days and south-facing slopes had a median shallow snow period of 29.5 days. The IQR for south facing slopes was also greater by 20.8 days, with south-facing slopes having an IQR of 50.8 days and north-facing slopes having an IQR of 30.0 days

Ground Temperature Response

After determining and comparing the zero-curtain periods, south-facing slopes had a shorter zero-curtain duration. The median zero-curtain duration for south-facing slopes was 20.5 days while the median zero-curtain duration for north-facing slopes was 87 days. Freezing onset also differed between slopes, with south-facing slopes having a median freezing onset date on 22 November 2025 and northern slopes having a median freezing onset date on 28 October 2025, with a difference of 25 days between freezing onsets.

Interannual comparison

Compared to previous water years, water year 2026 has a bigger variation in the last day of snow insulation across water years for both north and south facing slopes. Water year 2026 had an IQR 19 days larger than water year 2024 and 11 days larger than water year 2025 for north-facing slopes. For 2026, south facing slopes had an IQR 46 days larger than water year 2024 and 20 days larger than water year 2025. Furthermore, for north-facing slopes the first quartile date in 2026 was more than one month earlier compared to 2024 and one month earlier compared to

2025. For south facing slopes, the first quartile date in 2026 was more than two months earlier compared to 2024 and one month earlier than 2025. In 2026, south-facing slopes experienced a 65 and 10 days increase of full range of days compared to 2024 and 2025 respectively, while north-facing slopes experienced an 11 and 22 days increase of full range of days compared to 2024 and 2025 respectively.

Discussion

The results of this study show that slope aspect had an important influence on ground-temperature behavior, snow-insulation loss, and transitional snow conditions during WY2026. As hypothesized, south-facing slopes experienced earlier snow-insulation loss than north-facing slopes. However, earlier insulation loss did not necessarily correspond to earlier complete snow disappearance. As shown in Figure 6, south-facing slopes experienced longer periods of shallow or patchy snow conditions. North-facing slopes also exhibited longer near-zero ground-temperature periods than south-facing slopes. Finally, the greater spread of insulation-end dates among south-facing sites during WY2026 is consistent with increased sensitivity to low-snow conditions, although differences in site availability among years limit this interpretation.

The comparison among site characteristics showed that aspect and DAH had the clearest relationships with snow-insulation timing, each explaining approximately 41% of the observed variation. This is consistent with the role of slope orientation in controlling potential solar heating. In comparison, elevation explained only 13% of the variation, while slope, canopy cover, TPI, and modeled terrain exposure showed little individual relationship with insulation-end timing. The weak elevation relationship may partly reflect the relatively complex distribution of sites, where elevation covaries with aspect, vegetation, and terrain exposure rather than forming a simple elevational gradient. Similarly, the lack of a clear canopy or terrain-shading relationship does not indicate that these factors are unimportant, but rather that their independent effects were not detectable within this relatively small monitoring network.

The 31-day difference in median snow-insulation end date between north and south-facing slopes is consistent with the expected effect of slope aspect on incoming solar radiation. Previous research has shown that south-facing slopes generally receive greater solar energy (Lundquist & Flint 2006). As the snowpack becomes shallower, it loses its ability to insulate the ground, allowing ground temperatures to increase and exhibit greater daily fluctuations. In contrast, lower solar exposure on north-facing slopes allows deep, thermally stable snow to persist later into the spring. These differences likely contributed to the later median snow-insulation end date observed at north-facing sites.

Although the median insulation end date differed by 31 days between aspect groups, the median difference in final snow-presence date was only 6.5 days. This indicates that the loss of deep-snow insulation did not represent immediate snow disappearance, particularly on south-facing slopes. Instead, many south-facing sites entered an extended period of shallow or patchy snow cover. Greater solar exposure likely caused the continuous snowpack to become fragmented earlier, while isolated patches remained in locally shaded areas, depressions, or locations with greater initial accumulation..

Slope aspect also influenced near-zero ground-temperature behavior. North-facing slopes had a median near-zero period of 87 days, compared with 20.5 days on south-facing slopes. The longer duration at north-facing sites was likely related to the longer persistence of deep, insulating snow, which limited ground-temperature fluctuations and maintained temperatures close to 0°C. Earlier insulation loss on south-facing slopes exposed the ground to atmospheric and solar heating sooner, causing temperatures to move outside the near-zero range. However, these results should be interpreted carefully because a long near-zero temperature period may reflect both snow insulation and soil freeze–thaw processes. Ground temperature alone cannot confirm that active phase change occurred throughout the entire period. Therefore, the metric may be more accurately described as a near-zero ground-temperature duration.

A particularly important feature of WY2026 was the greater variability in snow-insulation end dates compared with previous water years. For north-facing slopes, the IQR increased to 30 days in WY2026, compared with 11 days in WY2024 and 19 days in WY2025. For south-facing slopes, the increase was even larger, reaching 50 days in WY2026 compared with 4 days in WY2024 and 30 days in WY2025. These results suggest that south-facing slopes appeared particularly sensitive, with some sites losing insulating snow very early while others retained it much later into spring.

Several limitations should be considered when interpreting these results. First, snow conditions were inferred from ground-temperature variability rather than measured directly at every site using continuous snow-depth observations. Although the same temperature-based classification was applied consistently across sites, the selected thresholds may misclassify days during periods of shallow, intermittent, or recently accumulated snow. Camera imagery provided some visual context, but incomplete camera records prevented continuous validation of the temperature-based classifications at all locations. In particular, the AP1 camera experienced data loss, and equipment disturbance and possible sensor damage at RG5 reduced confidence in measurements from that site.

The interannual comparison was also affected by differences in data availability. Rustlers Gulch sites were not monitored during WY2024, meaning that the number and composition of sites differed among water years. Some apparent interannual differences could therefore reflect changes in the monitoring network as well as changes in snow conditions. The total number of sites was also relatively small, particularly after separating locations into north and south-facing groups, which limits the strength and generalizability at a group-level comparison.

These differences in snow-insulation timing may have important hydrologic consequences. Earlier loss of insulating snow exposes the ground to atmospheric heating sooner and may alter the timing of soil thaw, infiltration, and snowmelt-water storage. In addition, the extended shallow and patchy snow periods observed at south-facing sites indicate that snowmelt does not occur uniformly across the landscape. Instead, snow-covered and snow-free areas can coexist for several weeks, potentially creating spatial differences in when meltwater becomes available to soils and streams. Although streamflow was not directly attributed to individual slopes in this study, these results demonstrate one mechanism through which topographic heterogeneity may contribute to variability between watershed-scale snowpack and runoff.

Future studies should include ground-temperature sensors at multiple soil depths to better distinguish snow insulation from soil freeze–thaw processes and to characterize the vertical progression of freezing and thawing. Continuous snow-depth measurements would also provide an independent validation of the temperature-based snow classification. Additional monitoring across a larger number of north- and south-facing sites and over multiple low- and high-snow years would help determine whether the strong aspect differences observed during WY2026 are consistent across a broader range of snow conditions. Finally, incorporating soil moisture, measured solar radiation, and streamflow observations could help determine how differences in snow-insulation timing translate into differences in infiltration, subsurface storage, and runoff generation.

Overall, this study demonstrates that slope aspect was strongly associated with differences in snow-insulation timing and near-surface ground-temperature behavior across the East River watershed. South-facing sites generally lost insulating snow approximately one month earlier than north-facing sites but experienced substantially longer shallow or patchy snow periods, resulting in much smaller differences in final snow disappearance. WY2026 also exhibited greater variability in insulation-end timing than the preceding two water years, particularly among south-facing sites. These results highlight the importance of representing local topographic heterogeneity when evaluating snowmelt timing in mountain watersheds, especially during low-snow years.

East River Study Sites

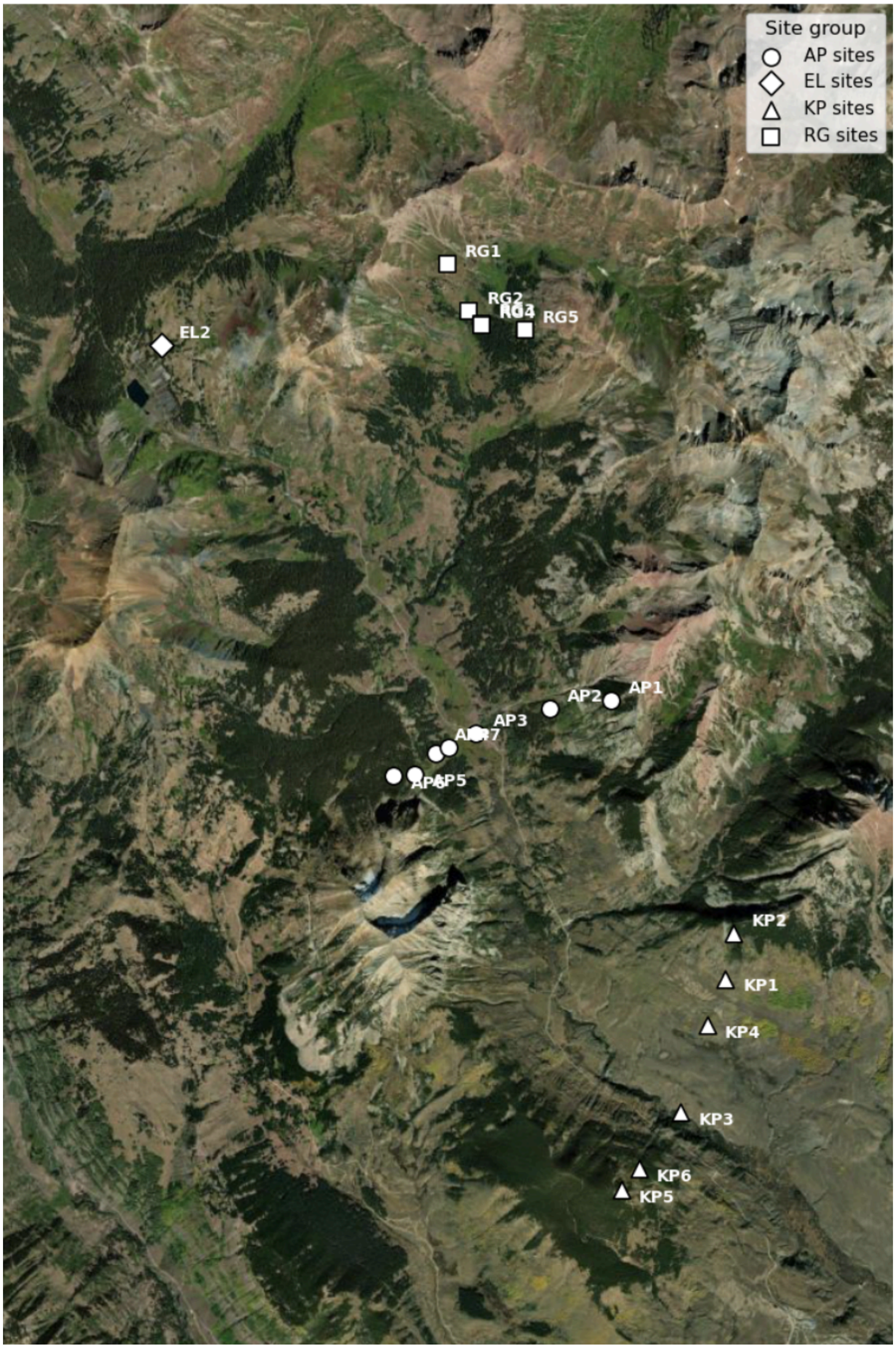

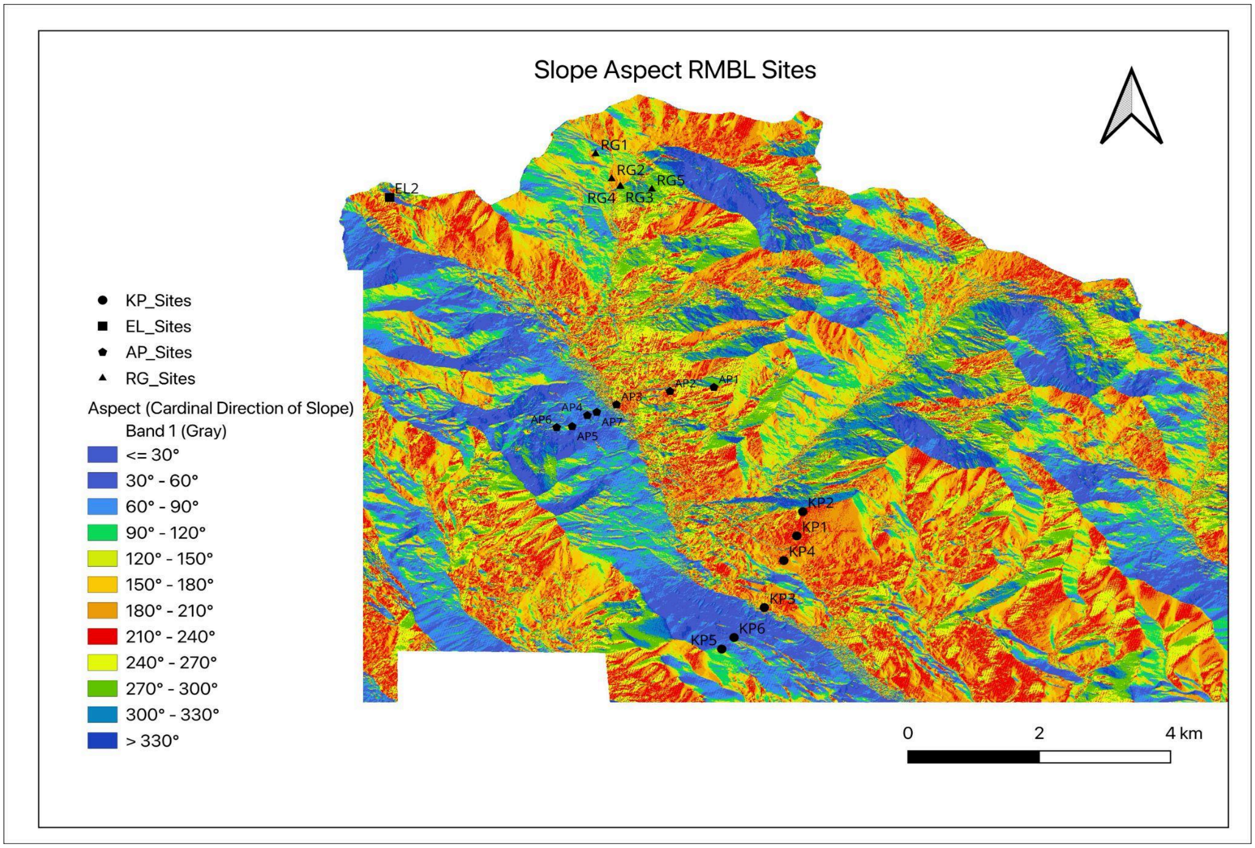

Figure 1. Overview of the study area and observation sites.

Figure 2. RG5 Sensor found unburied and approximately 5-8 cm above ground surface. Sensor still took temperature measurements.

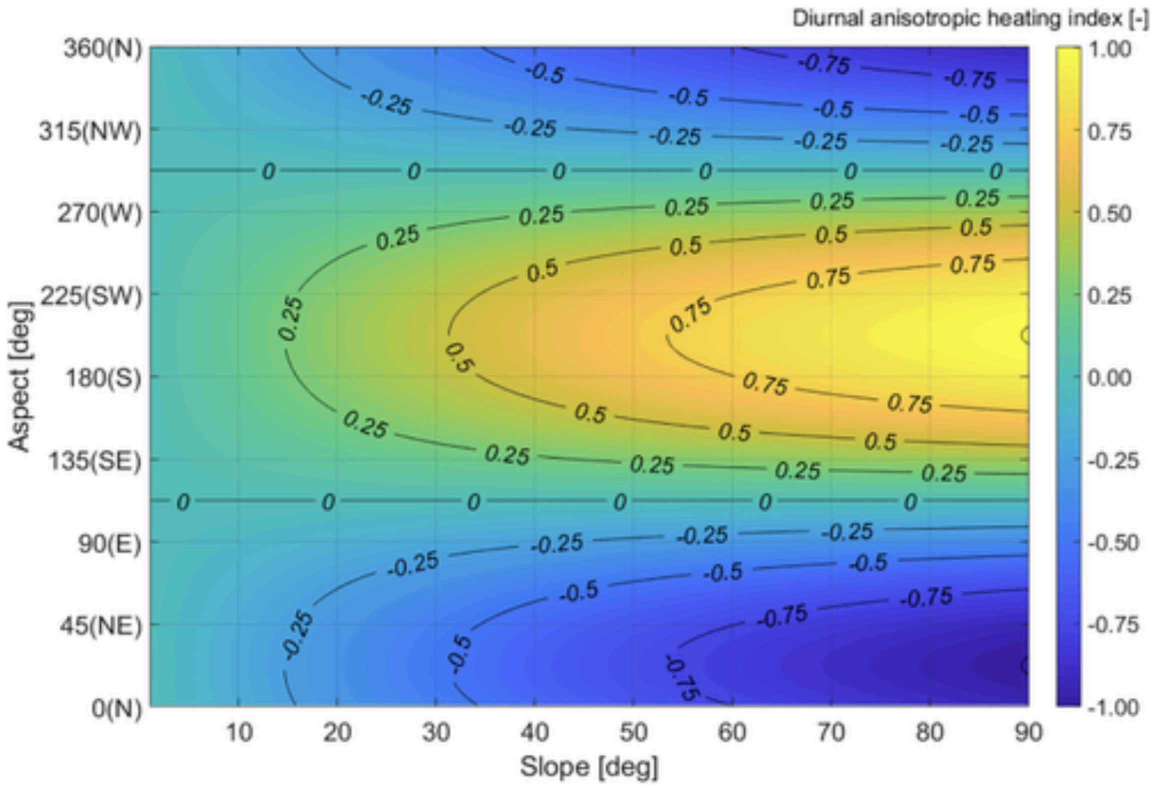

Figure 3. Diurnal anisotropic heating index variation as a function of slope and aspect. Figure reprinted from Cristea et al., 2017

Site	**Elevation(m)**	**Aspect(°)**	**Slope(°)**	**TPI (90m)**	**DAH**
AP1	3480	276.51°/North	35.91°	16.767	0.154
AP2	3099	222.26°/South	3.24°	8.809	0.053
AP3	2928	214.38°/South	2.77°	-0.572	0.047
AP4	3013	68.91°/North	11.42°	-3.331	-0.136
AP5	3167	86.87°/North	36.02°	2.538	-0.243
AP6	3238	18.46°/North	21.66°	10.632	-0.360
AP7	2951	58.84°/North	26.51°	-4.399	-0.349
KP1	3099	210.65°/South	21.79°	1.054	0.359
KP2	3282	210.54°/South	22.54°	3.510	0.369
KP3	2790	151.05°/South	1.68°	-12.137	0.018
KP4	2913	207.37°/South	17.14°	2.047	0.290
KP5	3285	56.94°/North	33.46°	20.205	-0.436
KP6	3129	44.83°/North	20.29°	8.099	-0.315
RG1	3404	128.88°/South	18.57°	6.673	0.088
RG2	3223	165.56°/South	6.59°	-1.810	0.091
RG3	3202	167.29°/South	17.07°	-4.830	0.237
RG4	3200	127.19°/South	2.59°	-6.096	0.011
RG5	3327	304.42°/North	28.57°	-2.928	-0.096
EL2	3425	13.86°/North	34.34°	6.719	-0.534

Table 1. Topographic Characteristics of study sites across East River watershed

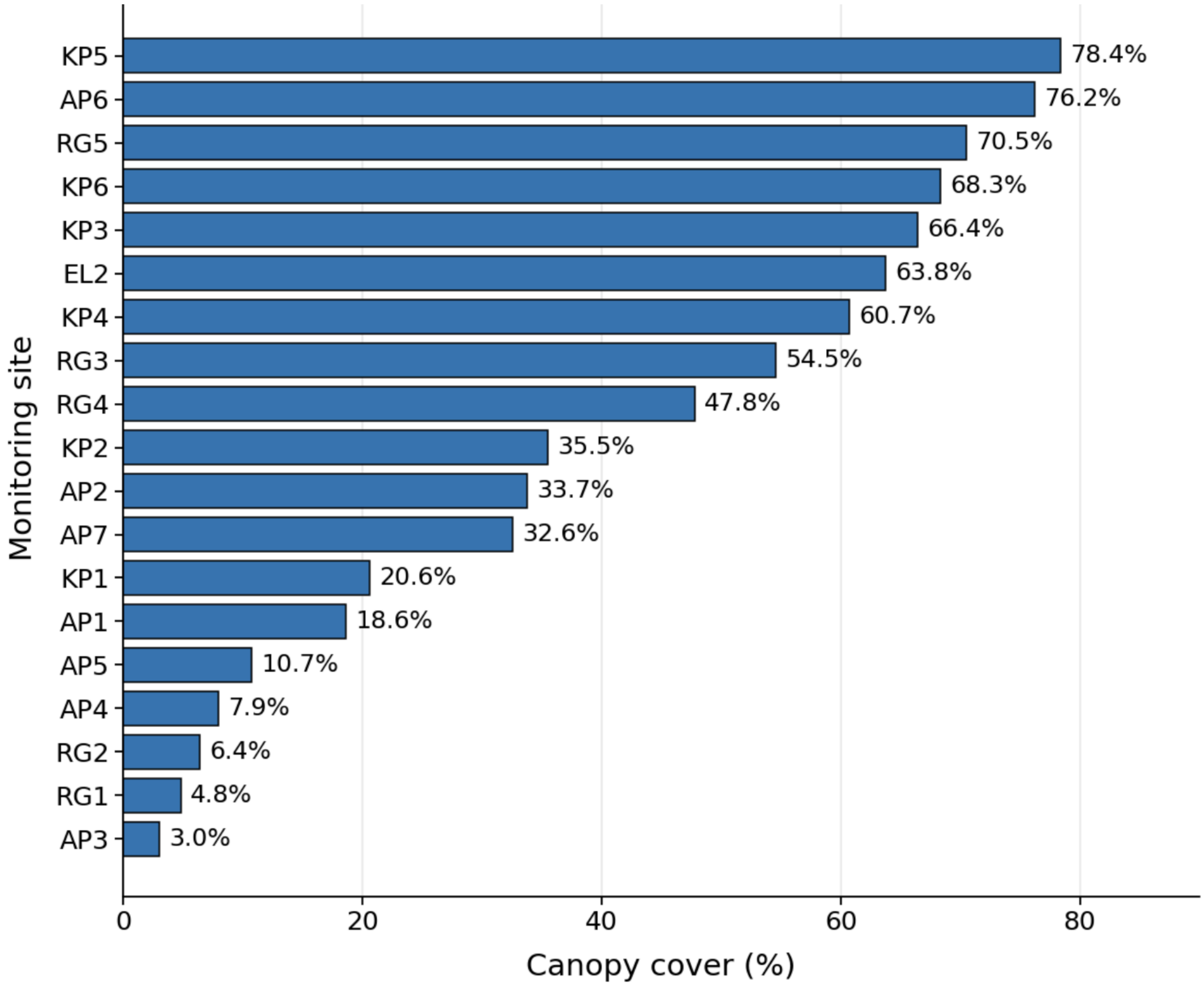

Figure 4. LiDAR-derived canopy cover at the 19 monitoring sites. Sites are ordered from highest to lowest canopy cover. Values represent the percentage of the 9 m raster cell occupied by canopy between 2 and 45 m above the ground surface.

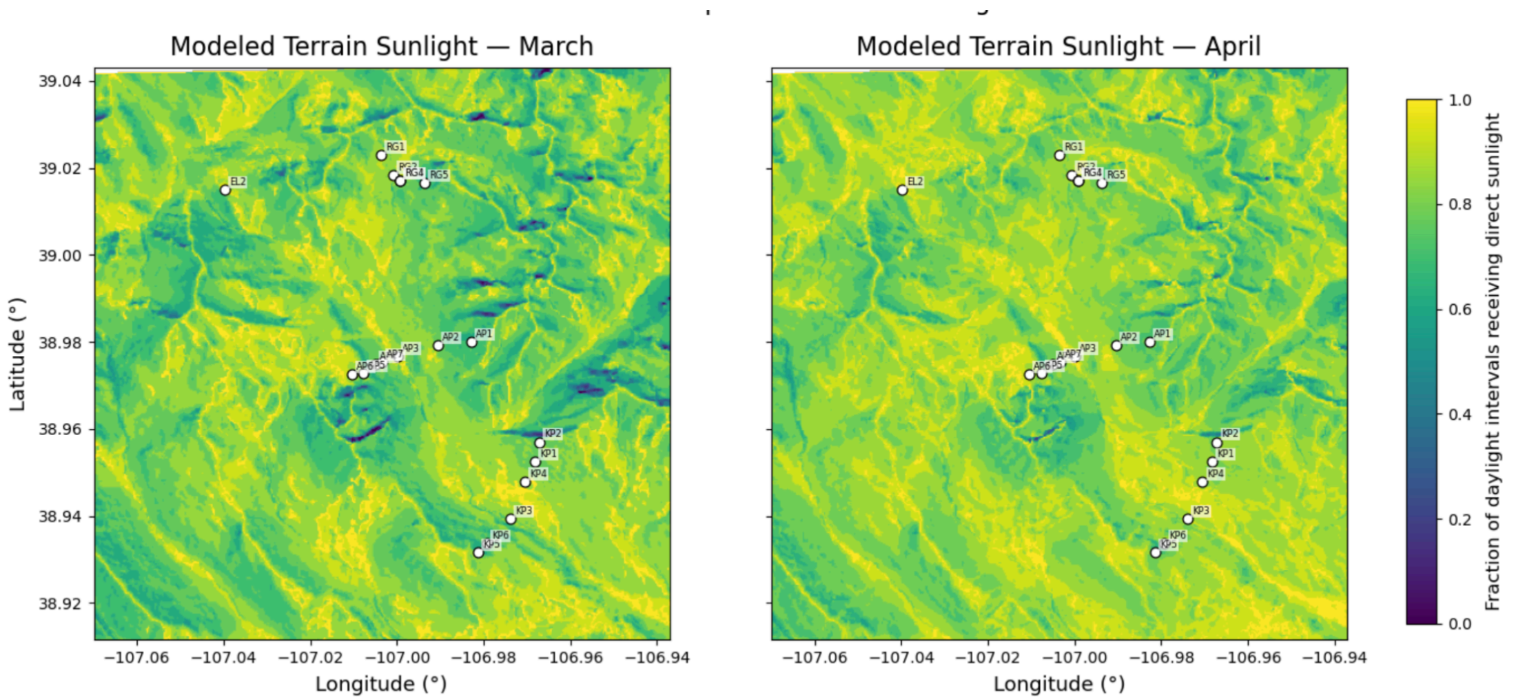

Figure 5. Monthly modeled direct-sun exposure at each monitoring site. Values represent the proportion of modeled daylight intervals during which direct sunlight was not obstructed by surrounding terrain on the representative monthly day.

Site Characteristic	R^2-value	p-value	Interpretation
Aspect	0.41	0.015	Strong cyclic relationship
DAH	0.41	0.003	Higher heating associated with earlier insulation loss
Elevation	0.13	0.13	Weak relationship
TPI, 30 and 90M	0.01-0.03	0.498/0.756	No clear relationship
Canopy cover	0.00	0.869	No clear relationship
Slope angle	0.01	0.636	No clear relationship
Terrain Exposure	0.00-0.05	0.378-0.798	No clear relationship

Table 2. Relationship between topographic characteristics of monitoring sites and snowmelt timing

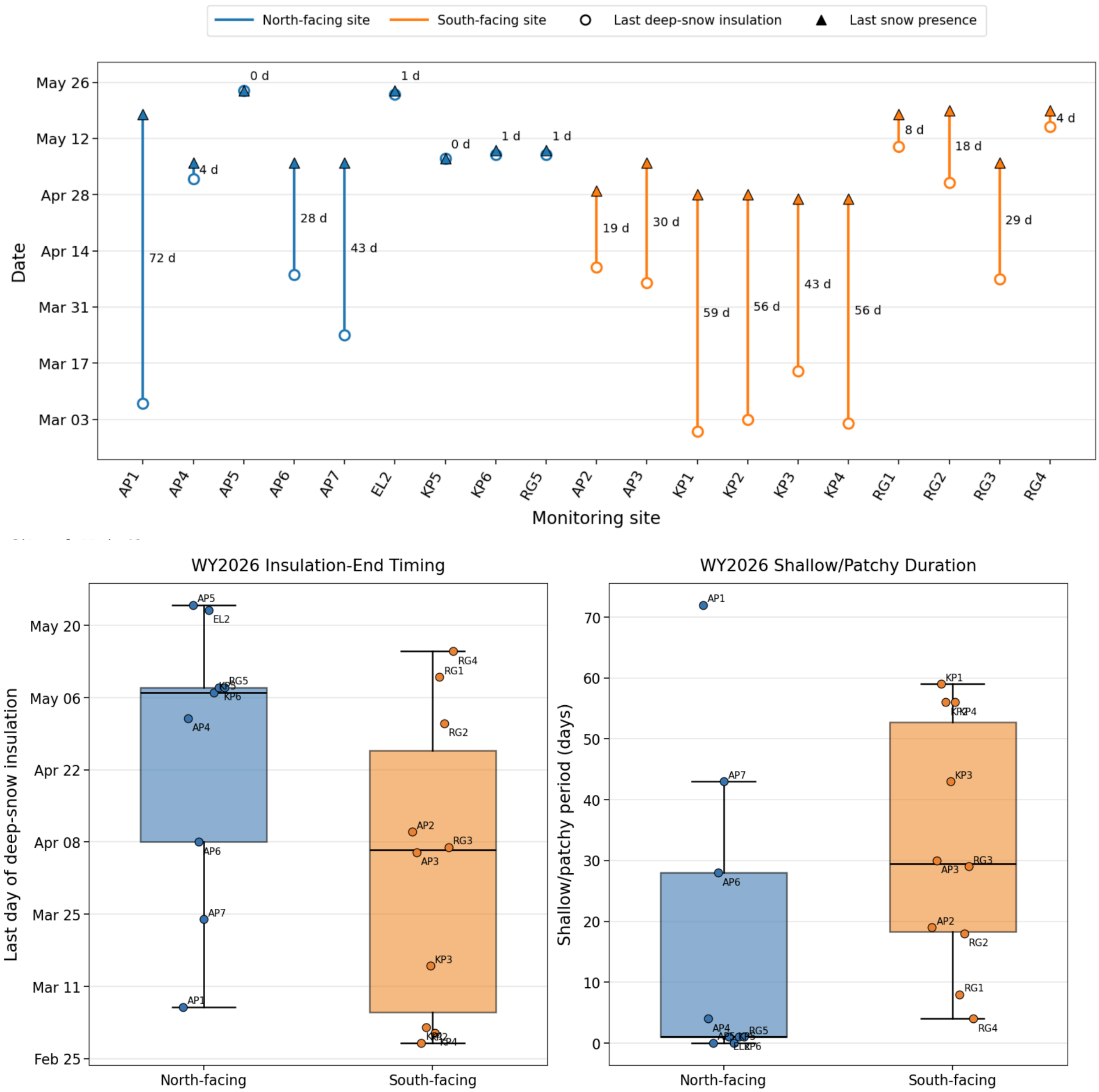

Figure 6. Snow-insulation loss and snow-disappearance timing at monitoring sites during Water Year 2026. *(a) Site-specific dates of final deep-snow insulation and final snow presence. (b) Distribution of last deep-snow insulation dates for north- and south-facing sites. (c) Distribution of shallow or patchy snow duration for north- and south-facing sites.*

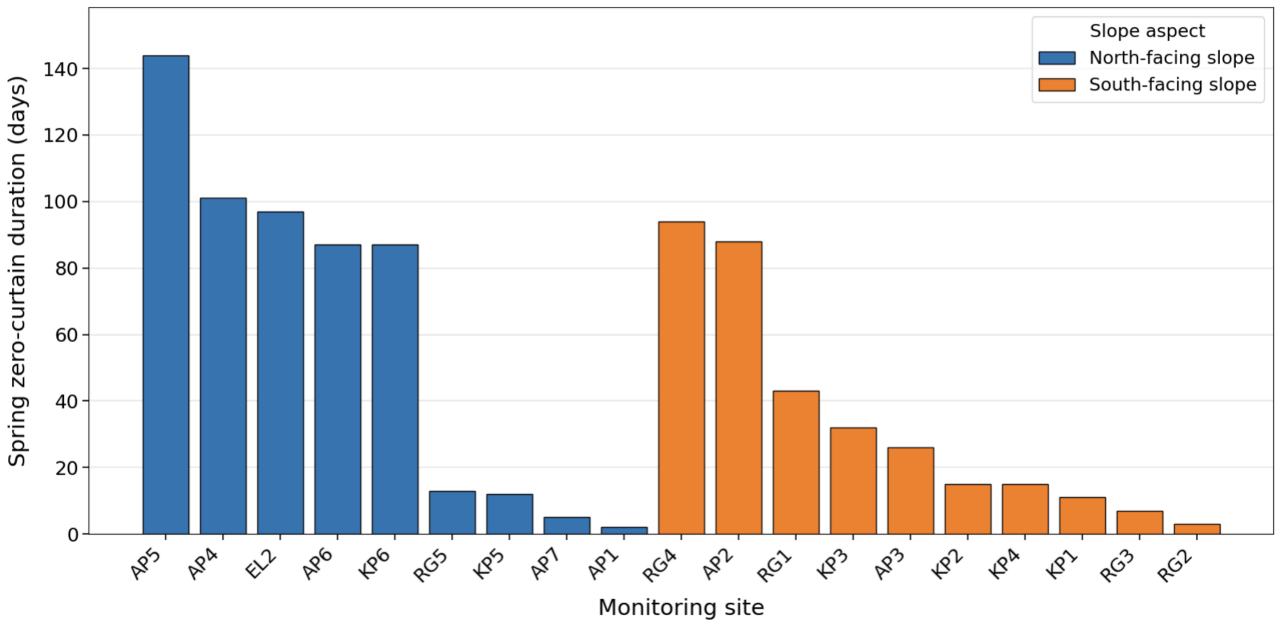

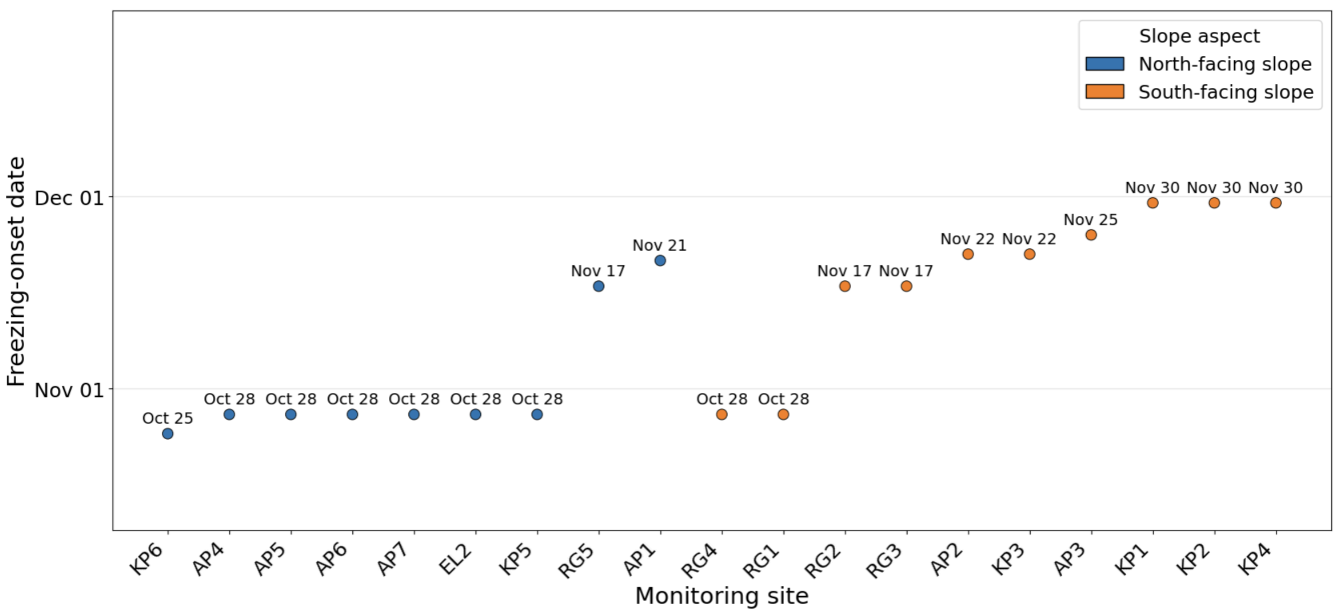

Figure 7. Ground-temperature behavior at north- and south-facing monitoring sites during Water Year 2026. *(a) Duration of the continuous near-zero ground-temperature period identified at each site.(b) Ground-freezing onset date at each site, defined as the first of three consecutive valid days with daily mean ground temperature below 0°C.*

Water year	Aspect	First Quartile Date	Third Quartile Date	IQR Days	Earliest Date	Latest Date	Full Range Days
2024	North	May 26	June 06	11	April 06	June 12	67
2025	North	May 09	May 28	19	April 05	May 31	56
2026	North	April 08	May 08	30	Mar 07	May 24	78
2024	South	May 12	May 16	4	May 12	May 24	12
2025	South	April 06	May 10	30	Mar 26	June 01	67
2026	South	Mar 06	April 26	50	Feb 28	May 15	77

Table 3. Distribution of last deep-snow insulation dates by water year and slope aspect. *First- and third-quartile dates represent the 25th and 75th percentiles, respectively. The interquartile range is the number of days between these two dates and represents the spread of the middle 50% of sites.*

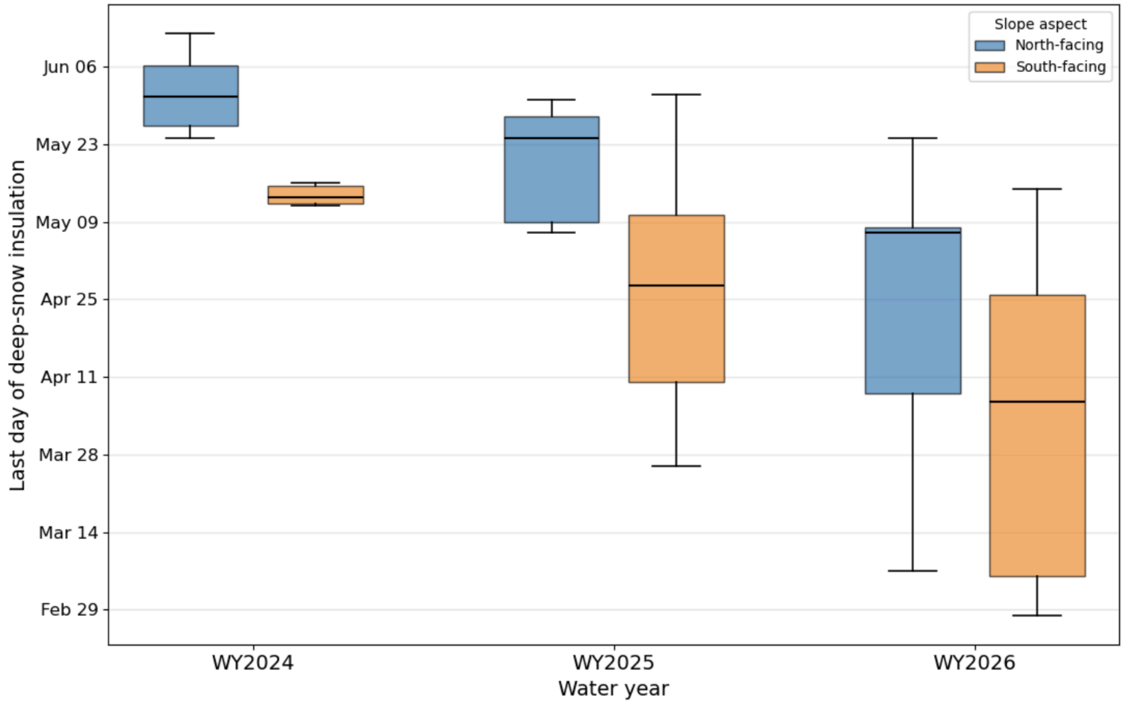

Figure 8. Interannual variation in snow-insulation and snow-disappearance timing by slope aspect. (a) Distribution of last deep-snow insulation dates at north- and south-facing monitoring sites during Water Years 2024–2026.. Blue represents north-facing sites and orange represents south-facing sites. Rustlers Gulch sites were included in Water Years 2025 and 2026 but were not available for Water Year 2024.

References:

Berghuijs, W. R., R. A. Woods, and M. Hrachowitz. “A Precipitation Shift from Snow towards Rain Leads to a Decrease in Streamflow.” Nature Climate Change 4, no. 7 (2014): 583–86. https://doi.org/10.1038/nclimate2246.

Cho, Eunsang, Carrie M. Vuyovich, Sujay V. Kumar, Melissa L. Wrzesien, Rhae Sung Kim, and Jennifer M. Jacobs. “Precipitation Biases and Snow Physics Limitations Drive the Uncertainties in Macroscale Modeled Snow Water Equivalent.” Hydrology and Earth System Sciences 26, no. 22 (2022): 5721–35. https://doi.org/10.5194/hess-26-5721-2022.

Cristea, Nicoleta C., Ian Breckheimer, Mark S. Raleigh, Janneke HilleRisLambers, and Jessica D. Lundquist. “An Evaluation of Terrain-Based Downscaling of Fractional Snow Covered Area Data Sets Based on LiDAR-Derived Snow Data and Orthoimagery.” *Water Resources Research* 53, no. 8 (2017): 6802–20. https://doi.org/10.1002/2017WR020799.

Falco, Nicola, Baptiste Dafflon, Haruko Wainwright, et al. “Integrated Imaging of above and below Ground Properties and Their Interactions: A Case Study in East River Watershed, Colorado.” n.d. Accessed June 19, 2026. https://dx.doi.org/10.1190/segam2018-2998456.1.

Fan, Y., M. Clark, D. M. Lawrence, et al. “Hillslope Hydrology in Global Change Research and Earth System Modeling.” Water Resources Research 55, no. 2 (2019): 1737–72. https://doi.org/10.1029/2018WR023903.

Fleck, John, and Brad Udall. “Managing Colorado River Risk.” Science 372, no. 6545 (2021): 885–885. https://doi.org/10.1126/science.abj5498.

Gordon, Beatrice L., Wade T. Crow, Alexandra G. Konings, David N. Dralle, and Adrian A. Harpold. “Can We Use the Water Budget to Infer Upland Catchment Behavior? The Role of Data Set Error Estimation and Interbasin Groundwater Flow.” Water Resources Research 58, no. 9 (2022): e2021WR030966. https://doi.org/10.1029/2021WR030966.

Kampf, Stephanie K., Stephen J. Burges, John C. Hammond, et al. “The Case for an Open Water Balance: Re-Envisioning Network Design and Data Analysis for a Complex, Uncertain World.” Water Resources Research 56, no. 6 (2020): e2019WR026699. https://doi.org/10.1029/2019WR026699.

Li, Dongyue, Melissa L. Wrzesien, Michael Durand, Jennifer Adam, and Dennis P. Lettenmaier. “How Much Runoff Originates as Snow in the Western United States, and How Will That Change in the Future?” Geophysical Research Letters 44, no. 12 (2017): 6163–72. https://doi.org/10.1002/2017GL073551.

Lundquist, Jessica D., and Alan L. Flint. Onset of Snowmelt and Streamflow in 2004 in the Western United States: How Shading May Affect Spring Streamflow Timing in a Warmer World. Journal of Hydrometeorology. December 1, 2006. https://doi.org/10.1175/JHM539.1.

Milly, P. C. D., and K. A. Dunne. “Colorado River Flow Dwindles as Warming-Driven Loss of Reflective Snow Energizes Evaporation.” Science 367, no. 6483 (2020): 1252–55. https://doi.org/10.1126/science.aay9187.

Modi, Parthkumar A., Eric E. Small, Joseph Kasprzyk, and Ben Livneh. Investigating the Role of Snow Water Equivalent on Streamflow Predictability during Drought. Journal of Hydrometeorology. October 20, 2022. https://doi.org/10.1175/JHM-D-21-0229.1.

Slater, Andrew G., David M. Lawrence, and Charles D. Koven. “Process-Level Model Evaluation: A Snow and Heat Transfer Metric.” The Cryosphere 11, no. 2 (2017): 989–96. https://doi.org/10.5194/tc-11-989-2017.

Sturm, Matthew, Michael A. Goldstein, and Charles Parr. “Water and Life from Snow: A Trillion Dollar Science Question.” Water Resources Research 53, no. 5 (2017): 3534–44. https://doi.org/10.1002/2017WR020840.

Vano, Julie A., Tapash Das, and Dennis P. Lettenmaier. Hydrologic Sensitivities of Colorado River Runoff to Changes in Precipitation and Temperature. Journal of Hydrometeorology. June 1, 2012. https://doi.org/10.1175/JHM-D-11-069.1.